NANO · MICRO small
www.small-journal.com

Self-Powered High-Voltage Recharging System for Removing Noxious Tobacco Smoke by Biomimetic Hairy-Contact Triboelectric Nanogenerator

Jianjun Zhang, Pengfei Chen, Lulu Zu, Jin Yang, Yanshuo Sun, Hao Li, Baodong Chen, and Zhong Lin Wang**

The most common size range of particulate matter (PM) in tobacco smoke is 1.0 to 5.0 microns; however, a high number of the most harmful PM is as small as 0.5 micron that is a serious threat to human health, and it is difficult to remove. There is an urgent need to develop a new purification technology for high-efficiency removing tobacco smoke with easily construction and low cost. Here, a method of self-powered high-voltage recharging system is demonstrated by designing biomimetic hairy-contact triboelectric nanogenerator (BHC-TENG) for long-lasting adsorption with a wide range from PM 0.5 to PM 10. The open-circuit voltage of BHC-TENGs reaches 8.42 KV, which can continuously charge injection to the melt-blown fabric, whose surface potential is able to maintain nearly 260 V level and create a uniform electrostatic adsorption field on the surface. This high-voltage recharging system reduces the concentration of PMs to World Health Organization (WHO) standards, maintaining the purification efficiency of PM 0.5– PM 10 persistently over 90%.

1. Introduction

Air pollution, as one of the major health risks around the world, is responsible for the premature death of seven million people each year.[1,2] In the last decade, the rapid modernization of industry and society has resulted in excessive emissions of harmful gases such as industrial emissions and vehicle exhausts.[3–6] In addition, second-hand smoke is also one of the most important pollution sources. As one of the harmful components of tobacco smoke, particulate matter (PM) is mainly composed of sulfate, nitrate, chloride, organic carbon, elemental carbon, iron, and calcium.[7,8] Generally, PMs are categorized according to the diameter of the particles, which ranges from several nanometers to tens of microns.[9] For example, PM 2.5 is defined as particulate matter with an aerodynamic diameter less than 2.5 microns.[3] Air purification technology for the removal of PM from atmospheric pollution is a viable option, such as simple filtration, nano adsorption, photocatalytic purification, and electrostatic precipitation.[10–15] Among these de-dusting approaches, electrostatic precipitation is widely used in industries and indoors. However, some drawbacks of this approach, including the requirement for an external high-voltage power and high cost, make it inappropriate for large-scale outdoor usage.

Nature holds enormous energy, and wind energy is a typical type.[16–19] Utilizing harvested energy from the environment to purify air, rather than the commercial electricity, is an ideal solution against the atmospheric pollution. Triboelectric nanogenerator (TENG), originating from the coupling effect of triboelectrification and electrostatic induction, is proved to be a cost-effective and eco-friendly technology to convert irregular mechanical energy into electrical energy,[20–24] especially for low frequency vibrational energy such as wind and wave energy.[25–29] Furthermore, the high open-circuit voltage is one typical characteristic of TENG, which can reach several thousand volts easily,[30–32] hence it is promising for removing PM from the atmospheric pollution using electrostatic effects.[33]

In this work, a practical and economical self-powered high-voltage recharging system is proposed for removing tobacco smoke in the air. A biomimetic hairy-contact triboelectric nanogenerator (BHC-TENG) was fabricated to generate a high voltage exceeding 8.42 KV, which allows the melt-blown cloth of the filter layer to maintain a constant high potential, ensuring excellent adsorption of PM 0.5–10 while greater safety than other high-voltage devices. After charging, the removal efficiencies of the high-voltage recharging system to PM 0.5 and

J. Zhang, J. Yang, Y. Sun, H. Li
College of Chemistry and Chemical Engineering
Center on Nanoenergy Research
Guangxi University
Nanning 530004, P. R. China

J. Zhang, P. Chen, L. Zu, J. Yang, Y. Sun, H. Li, B. Chen, Z. L. Wang
Beijing Institute of Nanoenergy and Nanosystems
Chinese Academy of Sciences
Beijing 101400, P. R. China
E-mail: chenbaodong@binn.cas.cn; zhong.wang@mse.gatech.edu

P. Chen, L. Zu, B. Chen, Z. L. Wang
School of Nanoscience and Technology
University of Chinese Academy of Sciences
Beijing 100049, P. R. China

B. Chen
Institute of Applied Nanotechnology
Jiaxing, Zhejiang 314031, P. R. China

Z. L. Wang
School of Materials Science and Engineering
Georgia Institute of Technology
Atlanta, GA 30332-0245, USA

The ORCID identification number(s) for the author(s) of this article can be found under https://doi.org/10.1002/smll.202202835.

DOI: 10.1002/smll.202202835

PM 1.0 both reach 90%, and that of PM 2.5, PM 5, and PM 10 all exceeded 98%. It is a novel application for TENG that is visualizing the process of the conversion of wind energy into high-voltage electrical energy to injection charge to enhance the electrostatic adsorption very nicely. The strategy of the proposed system is cost-effective and has great potential in commercial and practical applications for its diversified size and high efficiency, which helps to achieve the goals of environmental cleanliness and carbon neutrality.

2. Results and Discussion

2.1. Structure and Working Principle

The typical application scenario of the self-powered high-voltage recharging system in tobacco smoke was demonstrated in **Figure 1**a. A turbine vent shell made of 304 stainless steel is attached to the top of the smoking room and this construction has been proved to be very waterproof in our previous work.[34] The photograph of the internal structure is illustrated in Figure S1, Supporting Information. The turbine unit contains a self-powered high-voltage recharging system inside as shown in Figure 1b. The three rotors of BHC-TENG are connected by three acrylic tubes (the diameter of the acrylic tube is larger than that of the rotor), and they are fixed on the top of the turbine vent shell, so the rotors will rotate with the shell of the turbine vent; the three stators are fixed on the shaft of the turbine vent and they cannot rotate. The acrylic tube not only plays the role of connecting the rotors, but also plays a certain role in packaging. When the wind from any direction drives the shell of turbine vent to rotate, it not only removes hot or dirty air from the room but also drives the BHC-TENG to generate extremely high voltages. The negative electrode was connected to the copper-wire mesh shown in Figure 1c, and the positive electrode was connected to the microneedle array shown in Figure 1e. The melt-blown fabrics (Figure 1d) are attached to the surface of the copper wire mesh, ≈10 mm away from the microneedle array. A strong electric field is formed between the copper wire mesh and the microneedle array, in which the melt-blown fabric is polarized, resulting in a lower surface potential. As we all know, melt-blown fabric is a good air filter material, so it is widely used to filter particles in the air. However, melt-blown fabric is easy to fail in a humid or dirty environment, because the potential of the surface decreases or disappears. We continuously charge the melt-blown cloth by the method of corona polarization, so that the surface maintains a high potential and maintains a strong filtering function. The high-voltage power supply and tip discharge required for corona polarization, the high voltage generated by TENG is input into

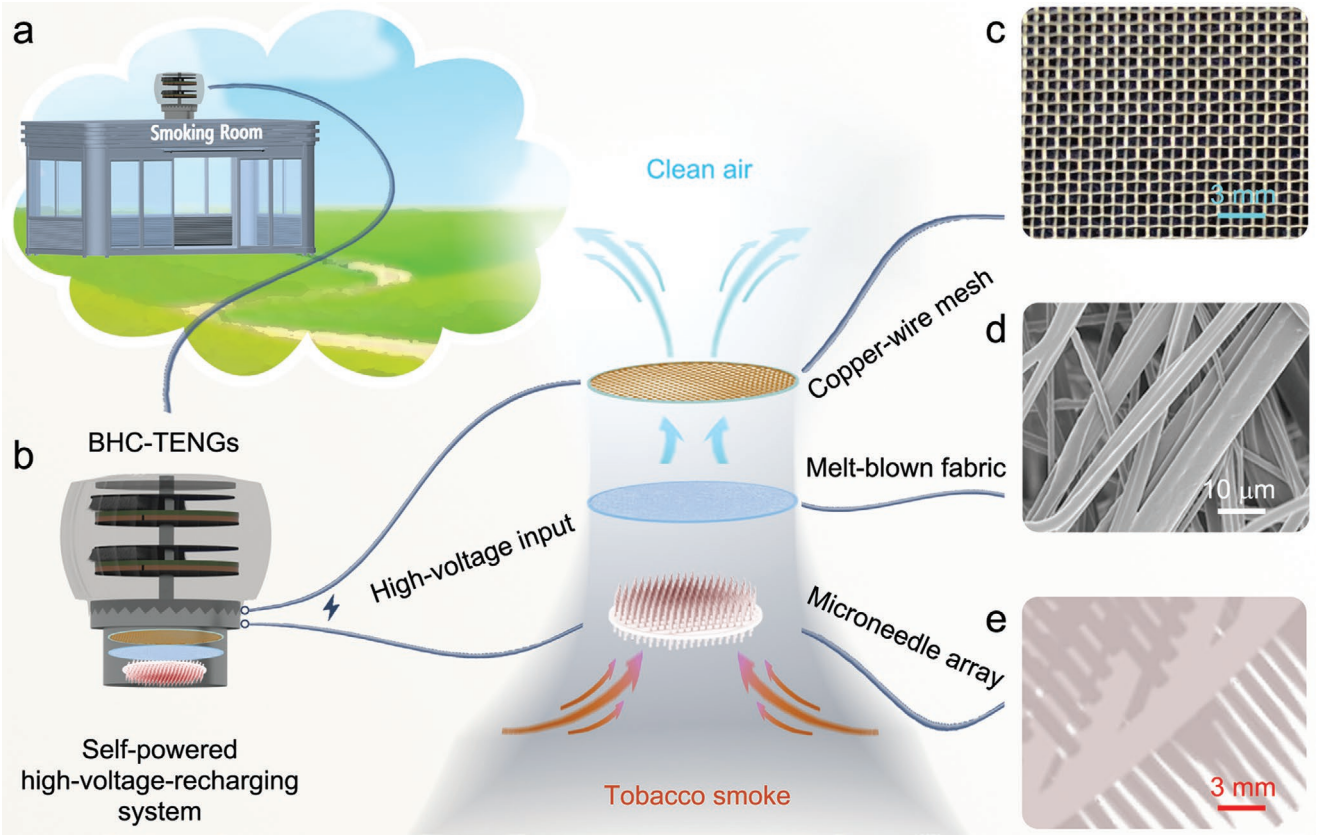

Figure 1. Application and architecture of BHC-TENG for integrating a self-powered high-voltage recharging system. a) The concept of self-powered high-voltage recharging proposed by using BHC-TENGs in the field of tobacco smoke purification. b) Illustrations of BHC-TENGs for harvesting wind energy and self-powered high-voltage recharging system for purifying air. c) An enlarged diagram of the copper-wire mesh, d) melt-blown fabric, and e) a microneedle array.

the microneedle array, the role of the microneedle array is to discharge the tip to the melt-blown fabric, and the copper mesh acts as the electrode of the melt-blown fabric.

The major working process of TENGs, such as the friction between polymer and metal, is mainly manipulated by sufficient contact to increase the surface charge density for better output performance. In this case, the great resistance between the friction layers not only makes it difficult to rotate the turbine vents, but also tends to cause mechanical wear in the relative motion. BHC-TENG operates in a biomimetic hairy-contact mode, which can solve the above problems. Figure S3, Supporting Information, shows the photograph and Scanning Electron Microscopy (SEM) images of the Fluorinated Ethylene Propylene (FEP) film surface after ≈5000 testing cycles. When rabbit hair is used as the friction layer of the TENG, it can maintain close contact and low friction state with other triboelectric materials during a long-term operation to ensure high output performance and low wear. **Figure 2**a shows the structural details of the BHC-TENG. The electrode disc with a diameter of 20 cm has a grid-shaped copper foil and FEP as a friction layer. Similarly, another acrylic disc with the same dimensions was prepared while its friction layer was rabbit fur. Fixing the electrode disc to the shaft of the turbine vent, the fur disc is fixed to the turbine vent shell. Driven by the breeze, the fur disc rotates together with the housing of the wind cap, creating a relative movement to the electrode disc fixed on the

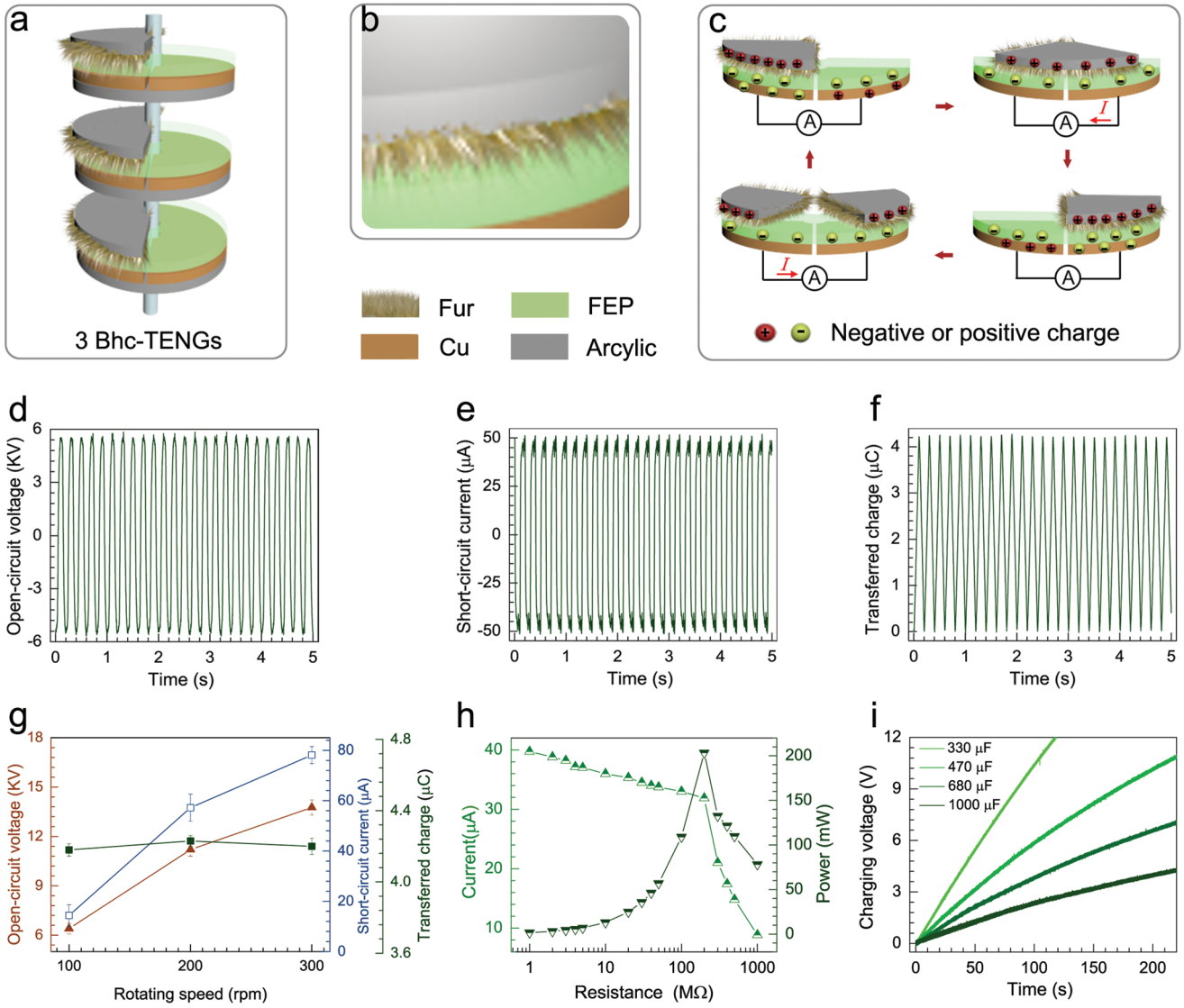

Figure 2. Architecture, mechanism, and output performance of BHC-TENGs: a) Material composition of BHC-TENGs, including electrode disk and fur disk. b) An enlarged schematic diagram of the material composition in the BHC-TENGs. c) Schematics of the four stages in one full electricity-generating cycle focusing on the charge distributions at the two sector-electrodes. d–f) The open-circuit voltage, the short-circuit current, and the transferred charges of BHC-TENGs with rotating speed of 200 r min^{-1}. g) The open-circuit voltage, the short-circuit current, and the transferred charges of BHC-TENGs with different rotating speed (data presented as mean ± SD, $n = 5$). h) Peak current and peak power of BHC-TENGs with respect to the load resistance with rotating speed of 300 r min^{-1}. i) Charging voltage on various capacitances for the motor-driven three BHC-TENG.

shaft. Figure 2b shows an enlarged schematic of the material composition in the BHC-TENGs. The working mechanism of BHC-TENG basing on the coupling effect of triboelectrification and electrostatic induction was shown in Figure 2c. The triboelectrification between the FEP film and furs generates negative charges on the FEP surface and positive electrostatic charges on the furs. Owing to the principle of conservation of charge, the total charge amounts on the furs and FEP are equivalent. The four states in Figure 2c represent a typical working cycle of BHC-TENG. With the relative rotation of the fur disk and electrode disk, free charges on the electrodes will be redistributed between two groups of electrodes through the external load to balance the change of potential difference. The induced periodically transferred charges between two groups of electrodes will produce alternating current output due to the periodic structure.

2.2. Electrical Characterizations of BHC-TENG

The output performance of BHC-TENG was optimized for a standardized dynamic torque measurement system as shown in Figure S2, Supporting Information. The transferred charges, short circuit current, and open circuit voltage of BHC-TENG with several common polymer materials against rabbit furs were presented in Figure S4, Supporting Information. The rotation speed of the fur disc was controlled to be 100 rpm and the dynamic torque was maintaining 0.2 N· m. As can be seen, the best output performance was obtained by rubbing the rabbit hair against the FEP film, due to the FEP film contains more F element which has easier access to electrons. We also tested the parallel connection of different numbers of BHC-TENGs, and it can be seen from Figure S5, Supporting Information, that the electrical output improves with the increasing in the number of BHC-TENG units. In addition, the number of grids of the electrodes also affects the output performance. Figure S6, Supporting Information, shows that the higher the number of grids, the lower the voltage output for the same area. However, the increase in the number of grids corresponds to an increase in frequency, so its current output is increased. To further demonstrate the output performance, three BHC-TENGs were connected in parallel and tested their output performance. Figure 2d–f shows the open-circuit voltage, short-circuit current, and transferred charges of three parallel-connected BHC-TENGs at a rotation speed of 200 rpm, which can reach 11.68 KV, 51.2 μA, and 4.25 μC, respectively. The open-circuit voltage and short-circuit current increase with the increasing speed of rotation as shown in Figure 2g. The open-circuit voltage and the short-circuit current reached to 13.86 KV and 78.35 μA, respectively, when the rotating speed increased to 300 rpm. The transferred charge is almost constant due to the contact area does not change. The electric power of three BHC-TENGs was investigated as shown in Figure 2h, in which the output power reaches a maximum value of 203.39 mW at a resistance of about 200 MΩ. When the rotating speed increased to 300 rpm, the charge density and power density of the fabricated BHC-TENG was 34.62 μC m^{-2} and 1656.62 mW m^{-2}, respectively. Figure 2i shows the self-powered recharging capability for various capacitors, in which the capacitor of 330 μF can be charged to 12 V in 118 s. For different capacitors of 470, 680, and 1000 μF, the voltage can arrive at 11, 7 and 4.3 V within 220 s, respectively.

2.3. Self-Powered High-Voltage Recharging System

It is well known that commercial melt-blown fabrics are often used to filter air due to their good charge storage stability at ambient temperature and humidity conditions. However, when melt-blown fabrics are exposed to high humidity environment, anisotropic particles in the atmosphere will compensate the charge on the fiber, due to the polar groups in the water molecules, resulting in a large loss of charge.[15] This developed self-powered high-voltage recharging system can solve this problem. The self-powered system can continuously inject charge to the melt-blown fabric, and the charge injection principle is shown in Figure S7, Supporting Information.[35,36] Under the action of the electric field applied by BHC-TENG, the melt-blown fabric and copper mesh electrodes are negatively and positively charged, respectively, with the same surface charge density. The schematic diagram of the high-voltage-recharging system working was shown in **Figure 3**a, and the photograph of BHC-TENG for wind energy harvesting measurement system as shown in Figure 3b. BHC-TENG can work at a minimum wind speed of 2.5 m s^{-1} as shown in Video S1, Supporting Information. Figure S8, Supporting Information, shows the output performance of the BHC-TENG, the open-circuit voltage, short-circuit current, and transferred charge were 3.54 KV, 2.12 μA, and 1.16 μC, respectively. It can be seen from Figure 3c that open-circuit voltage, short-circuit current, and transferred charge increase to 8.45 KV, 5.17 μA, and 1.43 μC, respectively, as the wind speed increases to 8 m s^{-1}. The output power of the BHC-TENG reached the maximum value of 6.6 mW at a resistance of about 1000 MΩ. Under the wind speed of 8 m s^{-1}, the charge density and power density of the fabricated BHC-TENG was 11.65 μC m^{-2} and 53.76 mW m^{-2}, respectively. Figure 3e shows the charging capability of three BCH-TENG to various capacitor at the wind speed of 8 m s^{-1}. The capacitor of 22, 33, and 47 μF can be charged to 10 V in 88, 137, and 168 s, respectively. For the capacitor of 100 and 220 μF, the voltage can arrive at 8.5 and 4.1 V within 300 s, respectively. Figure S9, Supporting Information, shows the open-circuit voltage of BHC-TENG under the different humidity, the humidity has little effect on its output performance. Furthermore, the BHC-TENG exhibits a good mechanical stability as shown in Figure S10, Supporting Information. It can continuously work for more than 60 000 cycles without obvious decrease. When melt-blown fabrics are exposed to dust particles for a longer duration, it results in a large loss of charge and the surface potential of the melt-blown fabric decreases. It can be seen from Figure S11, Supporting Information, that the surface potential of the melt-blown fabric decreased to almost 0 V when it was exposed to dust particles for 2 h. Figure 3f–i shows the surface potential of the melt-blown fabrics after corona charging by BHC-TENGs under the wind speed of f) 0, g) 4, h) 6 and i) 8 m s^{-1}. The surface potential of the melt-blown fabric also increases with increasing wind speed due to the open-circuit voltage of the BHC-TENG increases with increasing wind speed. The open-circuit voltage of BHC-TENG reached to 4.38 KV when the

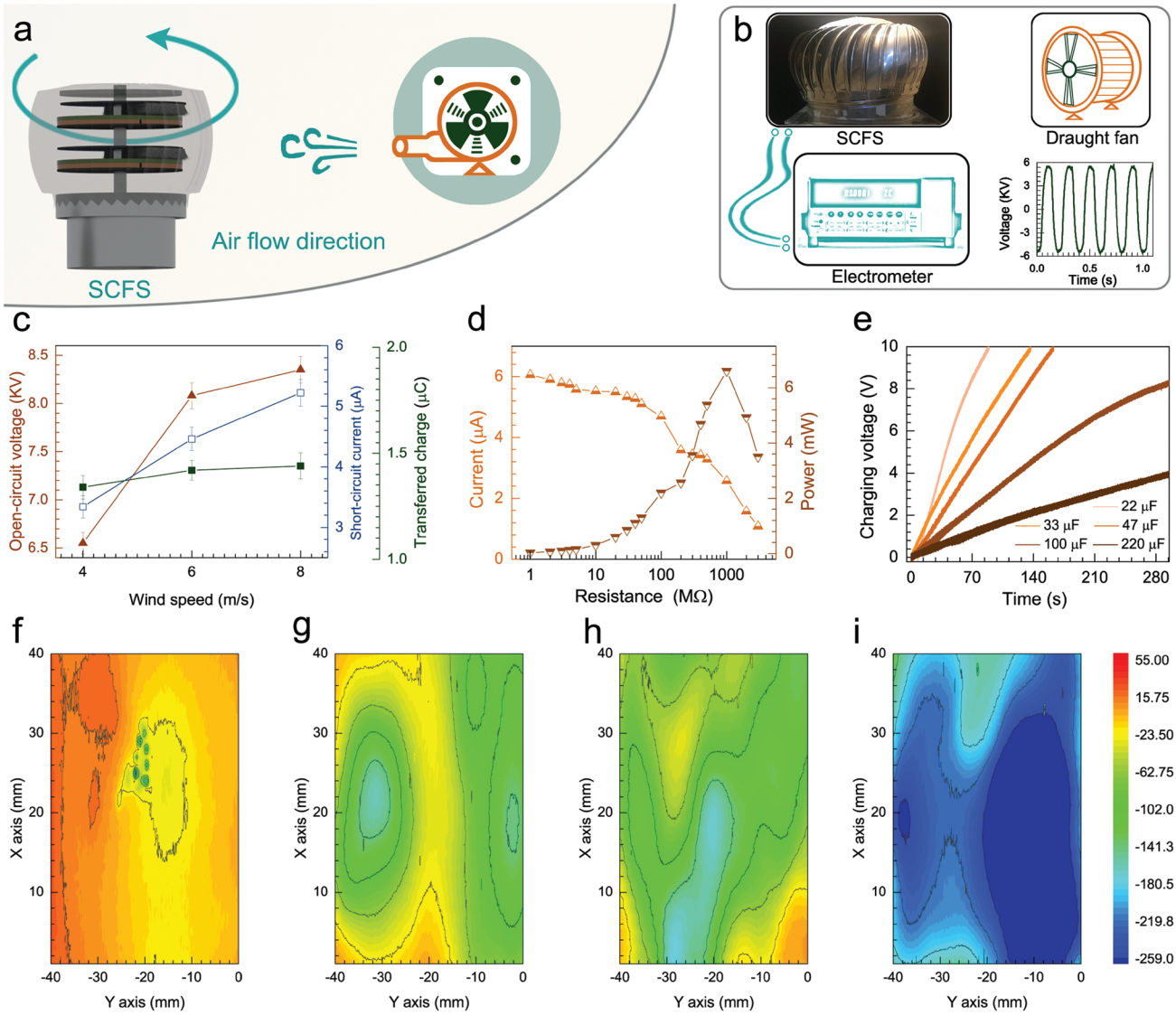

Figure 3. Application demonstrations of BHC-TENG for harvesting wind energy. a) Schematic diagram of BHC-TENG working. b) Schematic diagram of BHC-TENGs measurement system. c) The open-circuit voltage, the short-circuit current, and the transferred charges of BHC-TENGs under different wind speed (data presented as mean ± SD, $n = 5$). d) Peak current and peak power of BHC-TENGs with respect to the load resistance under wind speed of 8 m s^{-1}. e) Charging voltage on various capacitances for the wind-driven BHC-TENGs. f–i) The surface potential of the melt-blown fabric after corona charging by BHC-TENGs under the wind speed of 0, 4, 6, and 8 m s^{-1}.

wind speed increased to 8 m s^{-1}, the surface potential of the melt-blown fabric reaches up to nearly 260 V level.

An acrylic tube with a diameter of 25 cm was divided into two sections by the filter layer, with a particle counter placed at the left and filled with a certain concentration of cigarette smoke (**Figure 4**a), then the port is blocked with an acrylic plate. The right part is kept open to the outside for air exchange under external air flow conditions to verify the performance of the self-powered system (Figure 4b). From Figure 4c, different diameters of PM appear in the device, with relatively high concentrations of PM 2.5, PM 5.0 and PM 10.0, which are more hazardous to human health. Figure 4d compares the rate of decrease of PM 1.0 concentration with and without TENG drive. Without the BHC-TENGs driving, the PM 1.0 concentration decreases from 444.68 to 87.57 μg m^{-3} in 12 min, while with the driving of BHC-TENGs, PM 1.0 concentration decreases from 442.38 to 39.38 μg m^{-3}. It can be seen from Figure 4e that the concentration of PM 2.5 decreased significantly faster with three BHC-TENGs than without its driving. Without the BHC-TENGs driving, the PM 2.5 concentration decreases from 2891.09 to 1593.35 μg m^{-3} in first 2 min; while with driving of BHC-TENG, the PM 2.5 concentration decreases from 3458.87 to 1326.38 μg m^{-3}. This result shows that the purification efficiency was doubled compared to the case without BHC-TENGs, showing the effect of electrostatic field enhanced purification. The change curves of the residual concentration from PM 0.5– PM 10.0 driven by the BHC-TENGs and without are shown in Figure 4f. Not only for PM 2.5, it is clearly seen from

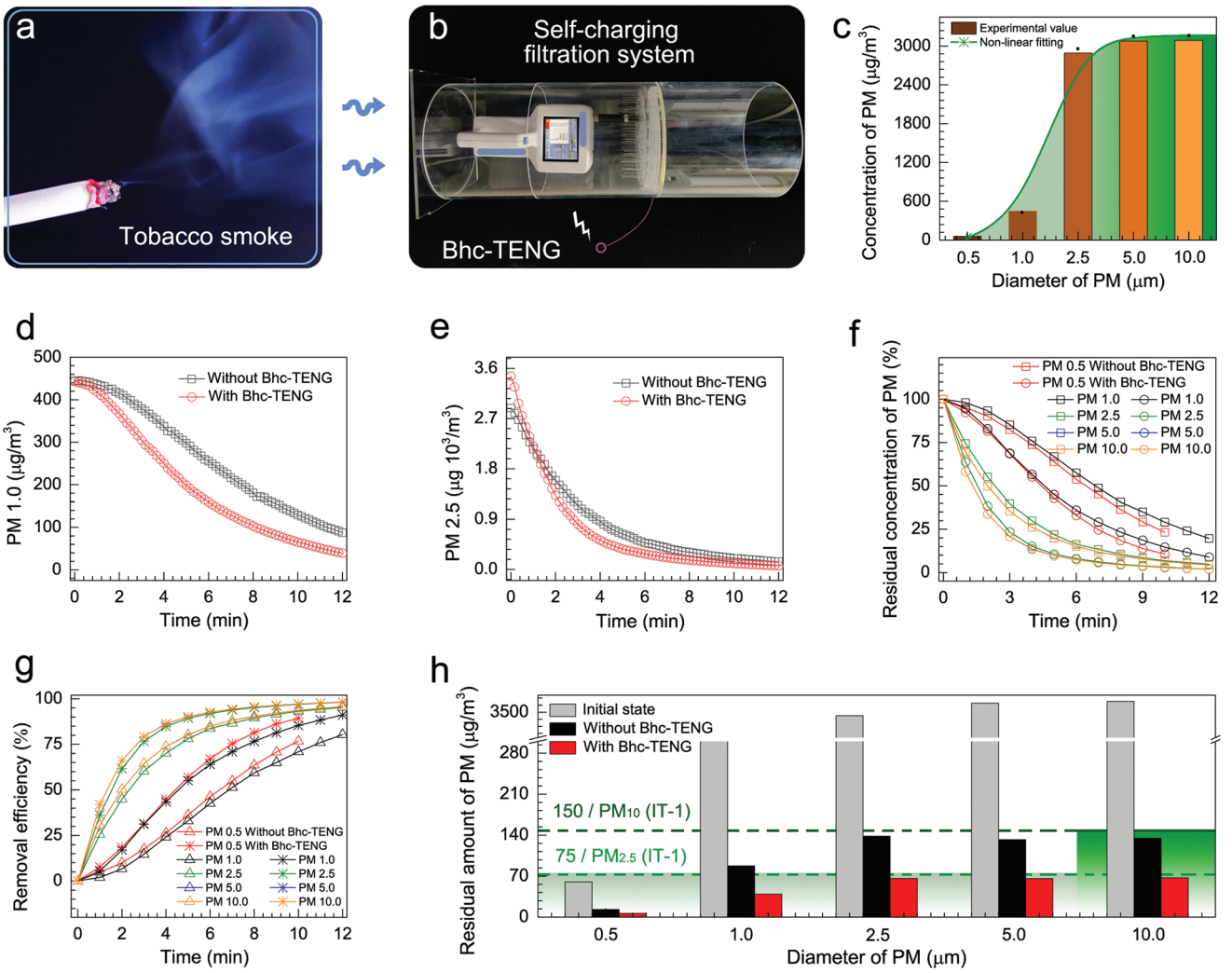

Figure 4. Performances of self-powered high-voltage recharging system based on the BHC-TENGs. a) Photograph of the tobacco smoke. b) Photograph of the self-powered high-voltage recharging system. c) The initial concentration of different diameter of PM in the container. d,e) The concentration changes in d) PM 1.0 and e) PM 2.5 degradation process with and without BHC-TENGs. f) The residual concentration changes of PM 0.5–10.0 in the decrease process with and without the BHC-TENGs. g) The removal efficiency of different PM with and without BHC-TENGs. h) The residual concentration of different PM at the end with and without BHC-TENGs.

Figure 4f that when the filter is driven by the BHC-TENGs, the concentration of all diameter of PMs but also decreases significantly faster than it was not driven. Besides, as shown in Figure 4g, the removal efficiency of the self-charging system for PM 0.5–10 maintains above 90%, which is significantly higher than without the BHC-TENGs driving. We calculate the efficiency according to the following formula:

$$\eta = \frac{C_0 - C}{C_0} \times 100\% \quad (1)$$

where C_0 and C represent the initial and final concentration (μg m^{-3}) of particles in the acrylic box, respectively. Figure 4h compares the results of the high-voltage-recharging system after 12 min of purification with and without driving. The results showed that the content of PM of various sizes decreased at the same time after the work of the self-powered system, which was reduced to the standard of the World Health Organization (WHO).[37] When the wind-driven turbine vent shell rotates, it will drive the work of BHC-TENG. The high voltage generated by BHC-TENG will be discharged through the tip of the microneedle array. The tip discharge will not only make the surface of the melt-blown fabric carry more charges and enhance its electrostatic adsorption, but also, the tip of the microneedle array discharges the surrounding particles at the same time, causing the particles to be charged and more easily adsorbed by the melt-blown fabric.

Figure 5a,b shows the schematic illustration for the high-voltage recharging system in smoking room. The volume of 0.216 m^3 acrylic box is connected to a 50 cm diameter turbine vent at the top. There is a 5 cm rectangular window on the side where this system is placed. We also studied the purification effect in the case of continuous PM release from the surrounding environment. A burning cigarette is placed at the

window of the acrylic box, and when the turbine vent rotates at the wind speed of 6 m s^{-1}, the internal air flows upward and exits the box through the unpowered air cap. Figure 5c shows the residual concentration of PM 0.5–10 change. The working process is shown in Video S2 and Figure S15, Supporting Information. It can be clearly seen that when the high-voltage-recharging system is driven by BHC-TENGs, the concentration of PM of various particle sizes inside the acrylic box is significantly lower than that without the TENG driving the high-voltage-recharging system. The tip of the microneedle array discharge not only makes the surface of the melt-blown fabric more charged and enhances its electrostatic adsorption ability, but also the tip of the microneedle array discharges the surrounding particles at the same time, so that the particles are charged and more easily adsorbed by the melt-blown cloth. Therefore, when the outside air enters the acrylic box through the melt-blown fabric, a lot of PMs in the air are adsorbed by the melt-blown fabric, resulting in cleaner air entering the acrylic box. Under the driving of three BHC-TENGs, the concentration of PM 2.5 is almost always lower than 50 μg m^{-3}; while without BHC-TENGs driving, the concentration of PM 2.5 decreases slowly, and can only be reduced to 50 μg m^{-3} after 175 s of purification. Because the air flow rate around the cigarette is unstable, resulting in the amount of cigarette smoke entering the acrylic box inside is also unstable, so the PM drop curve is not smooth. We also compared the effects of different air speeds on PM purification. As can be seen in Figure 5d, the remaining PM concentrations for various particle sizes are significantly lower at high wind speeds than at low speeds. The original is that when the wind speed is increased, the output voltage of the BHC-TENGs is higher and more effective for PM purification. Therefore, the removal efficiency of PM is higher at high wind speed than at low wind speed (Figure 5e). The removal efficiency of the high-voltage-recharging system for PM 2.5 reached to 64.67% and the residual concentration was 19.62 μg m^{-3}. Figure 5f shows the change of PM concentration of various particle sizes at different wind speeds, which is obvious as PM concentrations decreased faster at high wind speeds than at low wind speeds. To further test the performance of this self-powered system, we doubled the concentration of PM and lit two cigarettes at the same time and placed them at the window of the acrylic box. As can be seen from Figure 5g, the high-voltage-recharging system maintains a good purification performance even if PM concentration increases. Under the driving of three BHC-TENGs, the PM concentrations of all particle sizes were almost always lower than 50 μg m^{-3}. When the pollution source concentration added to three times, the residual concentration changes of PM0.5–10.0 in the removing process with and without BHC-TENGs were shown in Figure S12, Supporting Information. We can see that the residual concentration change was not obvious with or without BHC-TENGs. The changes before and after the purification of the melt-blown fabric were shown in Figure S13, Supporting Information. It is seen that the surface color of the melt-blown fabric becomes darker as the purification time increases. Figure S14, Supporting Information, shows the SEM images of the melt-blown fabric filtering PM before filtration (Figure S8a, Supporting Information) and after filtration for 4 h (Figure S8b, Supporting Information). We can see that the melt-blown fabric was clean in the Figure S8a, Supporting Information, and smooth, because the melt-blown fabric has adsorbed some PMs, so it looks rougher, as shown in Figure S8b, Supporting Information.

3. Conclusion

In summary, we proposed a unique self-powered tobacco smoke purification technology that is capable of effectively removing PMs in air, especially more harmful range of PM 0.5-2.5. The developed high-voltage recharging system based on the BHC-TENGs not only fully utilizes the wind energy, but also shows advantages in effectiveness, easy machining, easy maintenance, low cost, and light weight. With the BHC-TENGs driving, the removal efficiency of the high-voltage recharging system for PM 0.5–10 maintains over 90%, in which PM concentrations of all sizes in tobacco smoke were reduced to the WHO standard. More importantly, this system is self-powered and a standalone operation completely. This work demonstrates the high-voltage applications of BHC-TENG, which are expected to bring a great opportunity for removing PM hazard from tobacco smoke, opens new avenues for self-powered cleansing services in haze prevention and air purification, and may profoundly influence global air governance of public environment.

4. Experimental Section

Fabrication of BHC-TENG Unit: The TENG unit was composed of two parts: a fur disk and an electrode disk. For the electrode discs, the outer and inner diameters of the circular acrylic substrate were 200 and 30 mm, respectively. A copper foil was attached to one side of the acrylic, and a copper strip with a width of 6 mm was removed through the center of the circle, so the copper foil was divided into two parts and linked to the wires separately, and then a 30 μm thickness FEP film was adhered to the copper layer as a friction layer. For the fur disc, the same acrylic substrate as the electrode disc was affixed with rabbit fur with the area of one copper foil in the electrode disc. The wind was produced by a commercial air blower, and the wind speed was tested by an anemometer (THINRAD TA-1). The short-circuit current and transferred charges were measured by a current preamplifier (Keithley 6514 System Electrometer), while the output voltage directly produced by the BHC-TENG was measured using a mixed domain oscilloscope (HVP, Tektronix MDO3000s). Keithley 6514 electrometer was used as an ammeter in series with a resistor (100 GΩ) to measure the voltage of BHC-TENG, considering that the measured voltage exceeded the maximum range of the electrometer voltage range. The surface potential of the melt-blown fabric was measured by an electrostatic voltmeter (Trek 347). A 2D displacement platform (Zolix KSA100-11-X for each dimension) was used for scanning in the potential measurement. Then imported the data into origin software for plotting.

Fabrication of Self-Powered High-Voltage Recharging System: Fixing the microneedle at 1 cm, another on the acrylic plate, and connecting all the microneedles in series to form a microneedle array; then removed the excess acrylic to ensure the passage of air. The copper-wire mesh electrode was attached to the back of the melt-blown fabric and the microneedle array electrode was placed above the melt-blown fabric at a vertical distance of about 1 cm. With three parallel groups of BHC-TENG through the rectifier bridge, the positive electrode was connected to the microneedle array and the negative electrode was connected to the copper-wire mesh. The surface potential of the melt-blown fabric was measured by an electrostatic voltmeter (Model 344, Trek Company, USA). A handheld particle counter (Hand-held 3016-IAQ, Lighthouse,

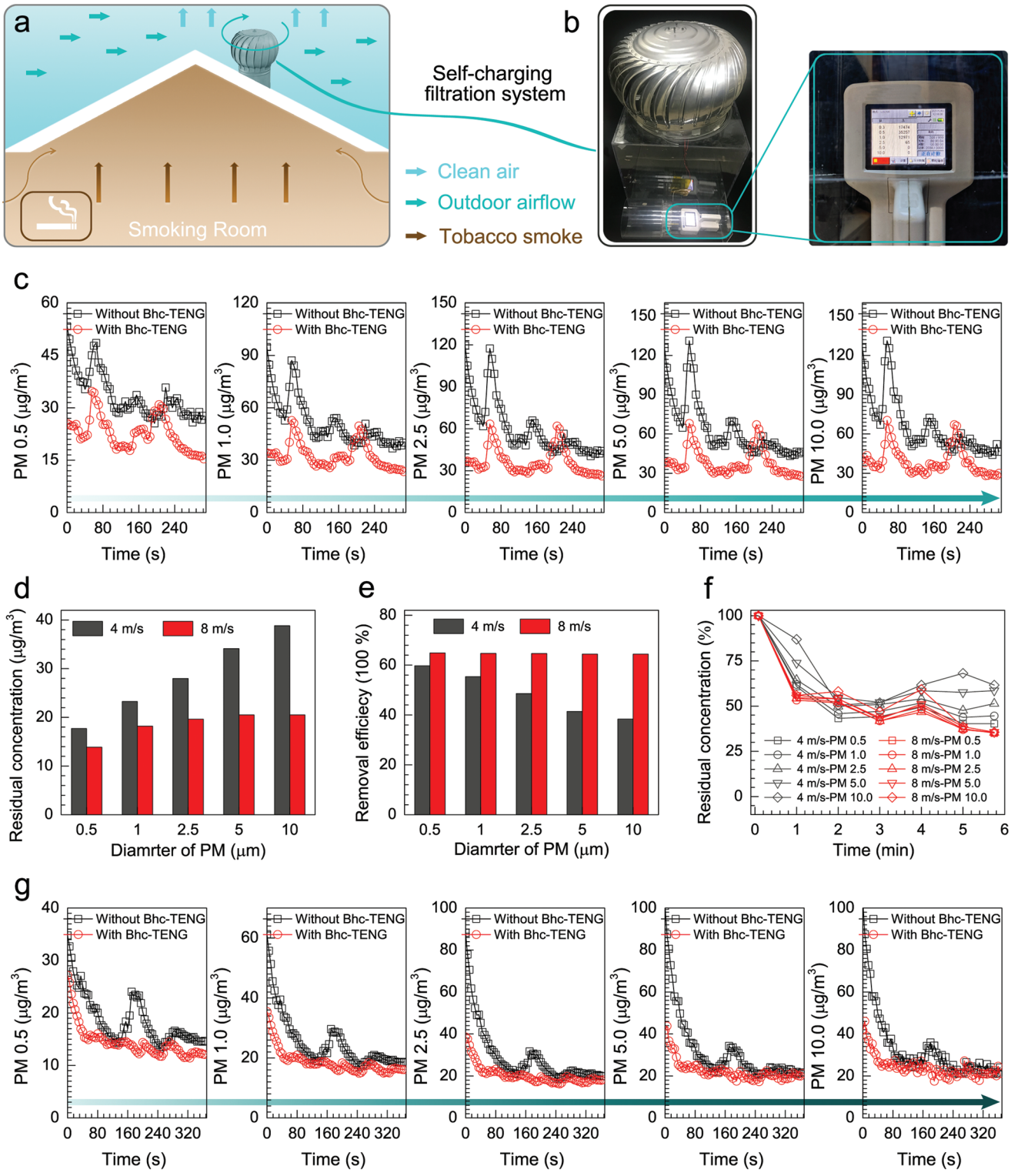

Figure 5. Applications of self-powered high-voltage recharging system for removing tobacco smoke with a wide range of PM 0.5–10. a) A schematic illustration showing the proposed the BHC-TENGs for self-powered high-voltage recharging in smoking room. b) Photograph of the self-powered high-voltage recharging system. c) The residual concentration changes of PM 0.5–10.0 in the removing process with and without BHC-TENG. d) The residual concentration of PM 0.5–10.0 through the high-voltage recharging system under different wind speeds. e) The removal efficiency of different diameters of PM. f) The percentage of residual concentration change of PM 0.5–10.0 in the removing process with and without BHC-TENGs. g) The residual concentration changes of PM 0.5–10.0 in the removing process with and without BHC-TENGs.

USA) was used to measure the PM concentration before and after purification. The removal efficiency was calculated by comparing the PM concentration before and after purification.

Statistical Analysis: All data were processed by Origin software. The residual concentration (%) was calculated according to the following formula:

$$\eta = \frac{C}{C_0} \times 100\% \quad (2)$$

where C_0 and C represent the initial and final concentration (μg m^{-3}) of particles in the acrylic box, respectively. The data of open-circuit voltage, the short-circuit current, and the transferred charges of BHC-TENGs were expressed as Means ± SD, the sample size for each statistical analysis was 5. Statistical analysis was performed by Origin (version 8.0).

Supporting Information

Supporting Information is available from the Wiley Online Library or from the author.

Acknowledgements

J.Z., P.C., and L.Z. contributed equally to this work. The authors acknowledge the support from the National Natural Science Foundation of China (Grant No. 52192610), and the National Key R & D Project from Minister of Science and Technology (2021YFA1201601).

Conflict of Interest

The authors declare no conflict of interest.

Data Availability Statement

The data that support the findings of this study are available from the corresponding author upon reasonable request.

Keywords

high-voltage recharging, particulate matter, purification efficiency, tobacco smoke, triboelectric nanogenerator

Received: May 7, 2022
Revised: July 4, 2022
Published online:

[1] A. Lai, M. L. Chang, R. P. O'Donnell, C. Zhou, J. A. Sumner, T. K. Hsiai, *Sci. Total Environ.* **2021**, *779*, 146464.
[2] D. E. Newby, P. M. Mannucci, G. S. Tell, A. A. Baccarelli, R. D. Brook, K. Donaldson, F. Forastiere, M. Franchini, O. H. Franco, I. Graham, G. Hoek, B. Hoffmann, M. F. Hoylaerts, N. Kunzli, N. Mills, J. Pekkanen, A. Peters, M. F. Piepoli, S. Rajagopalan, R. F. Storey, *Eur. Heart J.* **2015**, *36*, 83.
[3] C. B. Han, T. Jiang, C. Zhang, X. H. Li, C. Y. Zhang, X. Cao, Z. L. Wang, *ACS Nano* **2015**, *9*, 12552.
[4] P. Sadorsky, *Am. J. Econ. Sociol.* **2014**, *73*, 392.
[5] L. B. Lave, E. P. Seskin, *Science* **1970**, *169*, 723.
[6] Y. Feng, L. Ling, J. Nie, K. Han, X. Chen, Z. Bian, H. Li, Z. L. Wang, *ACS Nano* **2017**, *11*, 12411.
[7] J. H. Seinfeld, *Science* **1989**, *243*, 745.
[8] Y. Sun, G. Zhuang, Y. Wang, L. Han, J. Guo, M. Dan, W. Zhang, Z. Wang, Z. Hao, *Atmos. Environ.* **2004**, *38*, 5991.
[9] G. Q. Gu, C. B. Han, J. J. Tian, T. Jiang, C. He, C. X. Lu, Y. Bai, J. H. Nie, Z. Li, Z. L. Wang, *Nano Res.* **2018**, *11*, 4090.
[10] J. Xu, C. Liu, P. C. Hsu, K. Liu, R. Zhang, Y. Liu, Y. Cui, *Nano Lett.* **2016**, *16*, 1270.
[11] Y. Chen, S. Zhang, S. Cao, S. Li, F. Chen, S. Yuan, C. Xu, J. Zhou, X. Feng, X. Ma, B. Wang, *Adv. Mater.* **2017**, *29*, 1606221.
[12] H. M. Xiao, J. Y. Gui, G. J. Chen, C. P. Xiao, *J. Appl. Polym. Sci.* **2015**, *132*, 42807.
[13] X. Zhao, Y. Li, T. Hua, P. Jiang, X. Yin, J. Yu, B. Ding, *Small* **2017**, *13*, 1603306.
[14] T. C. Wu, Y. C. Chi, H. Y. Wang, C. T. Tsai, Y. F. Huang, G. R. Lin, *Sci. Rep.* **2017**, *7*, 11.
[15] Y. Bai, C. B. Han, C. He, G. Q. Gu, J. H. Nie, J. J. Shao, T. X. Xiao, C. R. Deng, Z. L. Wang, *Adv. Funct. Mater.* **2018**, *28*, 1706680.
[16] L. Zhang, B. Zhang, J. Chen, L. Jin, W. Deng, J. Tang, H. Zhang, H. Pan, M. Zhu, W. Yang, Z. L. Wang, *Adv. Mater.* **2016**, *28*, 1650.
[17] J. Chen, J. Yang, H. Guo, Z. Li, L. Zheng, Y. Su, Z. Wen, X. Fan, Z. L. Wang, *ACS Nano* **2015**, *9*, 12334.
[18] Y. Xie, S. Wang, L. Lin, Q. Jing, Z. H. Lin, S. Niu, Z. Wu, Z. L. Wang, *ACS Nano* **2013**, *7*, 7119.
[19] C. Ye, K. Dong, J. An, J. Yi, X. Peng, C. Ning, Z. L. Wang, *ACS Energy Lett.* **2021**, *6*, 1443.
[20] B. Chen, W. Tang, Z. L. Wang, *Mater. Today* **2021**, *50*, 224.
[21] W. Tang, C. Zhang, C. B. Han, Z. L. Wang, *Adv. Funct. Mater.* **2014**, *24*, 6684.
[22] P. Chen, J. An, R. Cheng, S. Shu, A. Berbille, T. Jiang, Z. L. Wang, *Energy Environ. Sci.* **2021**, *14*, 4523.
[23] J. Zhang, Y. Zheng, L. Xu, D. Wang, *Nano Energy* **2020**, *69*, 104435.
[24] W. Tang, T. Jiang, F. R. Fan, A. F. Yu, C. Zhang, X. Cao, Z. L. Wang, *Adv. Funct. Mater.* **2015**, *25*, 3718.
[25] P. F. Chen, J. An, S. Shu, R. W. Cheng, J. H. Nie, T. Jiang, Z. L. Wang, *Adv. Energy Mater.* **2021**, *11*, 2003066.
[26] J. Han, Y. Feng, P. Chen, X. Liang, H. Pang, T. Jiang, Z. L. Wang, *Adv. Funct. Mater.* **2021**, *32*, 2108580.
[27] T. Jiang, H. Pang, J. An, P. Lu, Y. Feng, X. Liang, W. Zhong, Z. L. Wang, *Adv. Energy Mater.* **2020**, *10*, 2000064.
[28] B. D. Chen, W. Tang, C. He, C. R. Deng, L. J. Yang, L. P. Zhu, J. Chen, J. J. Shao, L. Liu, Z. L. Wang, *Mater. Today* **2018**, *21*, 88.
[29] J. Zhang, Y. Sun, J. Yang, T. Jiang, W. Tang, B. Chen, Z. L. Wang, *ACS Appl. Mater. Interfaces* **2021**, *13*, 55136.
[30] Y. Liu, B. Chen, W. Li, L. Zu, W. Tang, Z. L. Wang, *Adv. Funct. Mater.* **2021**, *31*, 2104770.
[31] J. Cheng, W. Ding, Y. Zi, Y. Lu, L. Ji, F. Liu, C. Wu, Z. L. Wang, *Nat. Commun.* **2018**, *9*, 3733.
[32] A. Li, Y. Zi, H. Guo, Z. L. Wang, F. M. Fernandez, *Nat. Nanotechnol.* **2017**, *12*, 481.
[33] H. Guo, J. Chen, L. Wang, A. C. Wang, Y. Li, C. An, J.-H. He, C. Hu, V. K. S. Hsiao, Z. L. Wang, *Nat. Sustain.* **2021**, *4*, 147.
[34] J. J. Zhang, Y. S. Sun, J. Yang, T. Jiang, W. Tang, B. D. Chen, Z. L. Wang, *ACS Appl. Mater. Interfaces* **2021**, *13*, 55136.
[35] T. Zhou, L. Zhang, F. Xue, W. Tang, C. Zhang, Z. L. Wang, *Nano Res.* **2016**, *9*, 1442.
[36] Z. Wang, L. Cheng, Y. Zheng, Y. Qin, Z. L. Wang, *Nano Energy* **2014**, *10*, 37.
[37] A. Goshua, C. A. Akdis, K. C. Nadeau, *Allergy* **2022**, *77*, 1955.